ROYAL
AERONAUTICAL
SOCIETY

Handling qualities of fixed-pitch, variable-speed multicopters for urban air mobility

M. Bahr, M. McKay, R. Niemiec and F. Gandhi

Rensselaer Polytechnic Institute, Center for Mobility with Vertical Lift, Troy, NY, United States of America
E-mail: bahrm2@rpi.edu

Abstract

Optimisation-based control design techniques are applied to multicopters with variable-RPM rotors. The handling qualities and motor current requirements of a quadcopter, hexacopter and octocopter with equal gross weights (5,360N) and total disk areas (producing a 287N/m² disk loading) are compared in hover. For axes that rely on the rotor thrust (all except yaw), the increased inertia of the larger rotors on the quadcopter increase the current requirement, relative to vehicles with fewer, smaller rotors. Both the quadcopter and hexacopter have maximum current margin requirements (relative to hover) during a step command in longitudinal velocity. In yaw, rotor inertia is irrelevant, as the reaction torque of the motor is the same whether the rotor is accelerating or overcoming drag. This, combined with the octocopter's greater inertia as well as the fact that it requires 30% less current to drive its motors in hover, results in the octocopter requiring the greatest current margin, relative to hover conditions. To meet handling qualities requirements, the total weight of the motors of the octocopter and hexacopter is comparable at 13.5% weight fraction, but the quadcopter's motors are heavier, requiring 16% weight fraction. If the longitudinal and lateral axes were flown in ACAH mode, rather than TRC mode, the total motor weight of all configurations would be nearly identical, requiring about 13.5% weight fraction for motors (compared to 7–9% weight fraction from hover torque requirements).

Nomenclature

ACAH	attitude command attitude hold
B	motor viscous loss coefficient, Nms
C_T	rotor thrust coefficient
DRB	disturbance rejection bandwidth
DRP	disturbance rejection peak
eVTOL	electric vertical takeoff and landing
i	motor current, A
I_{rotor}	rotor inertia, kg m²
IL	inner loop
K_e	motor back-EMF constant, Vs/rad
K_t	motor torque constant, Nm/A
L	motor inductance, H
M_u	longitudinal speed stability derivative, rad/ms
N_{rotors}	number of rotors
OL	outer loop
Q	motor torque, Nm
Q_A	rotor aerodynamic torque, Nm
RCDH	rate command direction hold
R	rotor radius, m

R_m	motor resistance, Ω
TRC	translational rate command
UAM	urban air mobility
V	motor voltage, V
W_{eng}	motor weight, kg

Greek symbol

Ψ_k	Azimuthal position of kth rotor, rad
Ω	rotor speed, rad/s^2
$\dot{\Omega}$	rotor acceleration, rad/s^2

1.0 Introduction

Electric Vertical Takeoff and Landing (eVTOL) aircraft are the centrepiece of Urban Air Mobility (UAM). The simplicity of electric drive systems has lowered the barriers to entry into this new space, resulting in a proliferation of new designs by both well established and new VTOL manufacturers. The simplest eVTOL design is the scaled-up multicopter, such as the Volocopter 2X or the Airbus CityAirbus, where lift and propulsive thrust are produced by several rotors distributed across the airframe. Other eVTOL archetypes include tiltrotors, such as the Bell Nexus or Joby S4, and "lift+cruise" vehicles, such as the Wisk Cora and the Aurora Flight Sciences PAV.

As mentioned, all of these proposed vehicles utilise multiple rotors, and some more complex configurations operate using tilting or ducted rotors. A benefit of lift+cruise and some tiltrotor aircraft, such as the Joby S4 and Aurora PAV, is that use of a wing in forward flight reduces rotor loading and improves efficiency. While use of ducted rotors has the potential to improve rotor thrust and decrease noise, additional research is needed regarding implementation for UAM applications [1].

Recently, considerable attention has been given to the handling qualities of eVTOL aircraft for UAM applications. Many of these multi-rotor eVTOL aircraft use fixed-pitch, variable-RPM rotors. While the simplicity of these rotors is attractive, their inability to rapidly generate thrust as rotor size (and inertia) increases can become a serious impediment. Recent studies by Walter et al. [2, 3] suggest that while 0.3–1.2m (1–4) diameter rotors would have satisfactory handling qualities, 1.8 and 2.4m (6 and 8) diameter rotors (typical on manned-size eVTOL aircraft) would struggle to meet Level 1 handling qualities (due to saturation of motor power). However, the controllers used in Refs [2] and [3] were not designed considering a complete set of handling qualities requirements. Other studies by Malpica and Withrow-Maser [4] and Niemiec et al. [5] compare the use of fixed-pitch, variable-RPM rotors to variable-pitch rotors on multi-rotor eVTOL aircraft. Malpica and Withrow-Maser [4] found that variable-RPM controlled multicopters were unable to meet Level 1 handling qualities if current constraints were applied to the ESCs. The comparisons made by Niemiec et al. [5] showed that both variable-pitch and variable-RPM rotors required peak current for yaw rate step commands.

The present study uses the optimisation-based control design software CONDUIT® [6] to develop controllers for 5,360N (1,200lb) gross weight multi-rotor eVTOL aircraft, where actuator activity is minimised while meeting a set of handling qualities based on ADS-33E-PRF [7] specifications. These techniques have long been used on conventional VTOL aircraft [8], and have also been applied to small eVTOL aircraft in recent years [9–11]. CONDUIT® is used to optimise inner loop and outer loop control laws on a 5,360N quadcopter, hexacopter and octocopter, each having the same total disk area (and 287N/m^2 disk loading). This allows a comparison of the three aircraft (ranging from the quadcopter with the largest, highest-inertia rotors to the octocopter with the smallest, lowest-inertia rotors) in terms of their ability to execute manoeuvres and reject gusts. Rather than assume a particular actuator, and determine whether it is sufficient to meet handling qualities requirements, the motor current constraint is neglected. After optimising for minimum actuator activity, the commanded current during different manoeuvres and gust rejections will be used to determine the minimum motor size to meet handling qualities specifications.
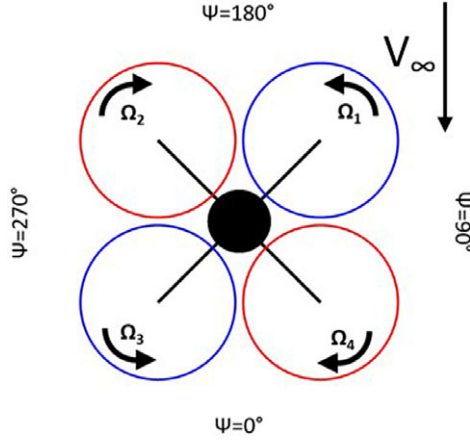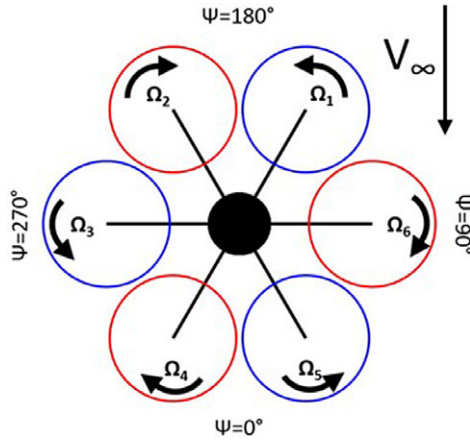
Figure 1. *Quadcopter*

Figure 2. *Hexacopter*

2.0 Platform

2.1 Aircraft model

Three different aircraft configurations are considered, multicopters with four, six and eight rotors. All three aircraft fly in an edge-first orientation, with two leading rotors, shown in Figs 1–3. In order to solve the six rigid-body equations of motion, six trim variables, comprised of multi-rotor speeds and the aircraft pitch and roll attitudes are required. The primary control modes are defined in multi-rotor coordinates [12], and the multi-rotor coordinate transform (Equation (1)) provides the individual rotor speeds. The parameter Ψ_k represents the azimuthal rotor position, with $0°$ at the aft of the aircraft (Figs 1–3). Defining the control modes in multi-rotor coordinates is beneficial because it decouples the aircraft dynamics. There are four primary, independent multi-rotor control modes for the configurations, Ω_0, Ω_{1s}, Ω_{1c} and Ω_d. Ω_0 represents a uniform increase in individual rotor speed, which regulates the vertical axis. Ω_{1s} increases the rotor speed on the right of the aircraft and decreases the rotor speed on the left of the aircraft, providing roll control. Ω_{1c} provides pitch control by increasing the speed of the rear rotors while decreasing the speed of the front rotors, causing a nose-down moment. The differential mode, Ω_d, increases and decreases alternating rotor speed about the aircraft azimuth, resulting in a nose-right yaw moment (in steady-state operation). For the hexacopter and octocopter, there are additional, reactionless multi-rotor control modes, which are not utilised.
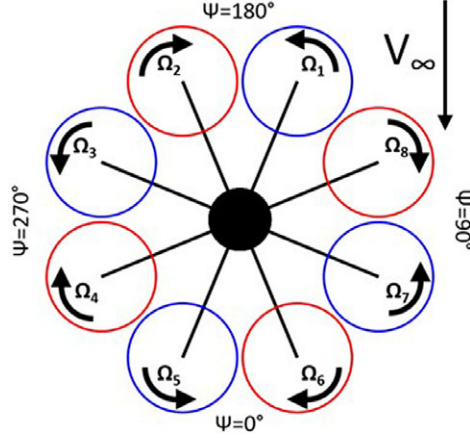
Figure 3. *Octocopter*

$$\Omega_k = \Omega_0 + \Omega_{1s} \sin \Psi_k + \Omega_{1c} \cos \Psi_k + \Omega_d(-1)^{k-1} \tag{1}$$

The three different aircraft all share disk loading of 287N/m^2 and disk area equal to a single, 2.44m radius rotor. Shared aircraft parameters are shown in Table 1, and the parameters that change across configurations are the number of rotors, rotor radius, and boom length, which are tabulated in Table 2. The boom length is chosen to maintain a 10% rotor radius tip-to-tip separation. While each aircraft is geometrically symmetric, an important distinction between the configurations is the pitch inertia (I_{yy}) is larger than the roll inertia (I_{xx}). The aircraft inertia in this study is scaled from the NASA concept quadcopter, which has been previously published [13].

2.2 Flight dynamics model

The rigid-body dynamics of each configuration are evaluated using the Rensselaer Multicopter Analysis Code (RMAC [14]). RMAC is a physics-based code that calculates the aircraft accelerations by summation of forces and moments at the aircraft centre of gravity. The rotor forces and moments are calculated using blade element theory, with a 3x4 Peters-He finite-state dynamic wake model [15]. Previously, RMAC has been validated using data from both flight tests [16] and wind tunnel tests [17], however, test data does not exist for aircraft at the scale presented in this study. Presently, RMAC is used to identify trim conditions for the aircraft, as well as linearise the aircraft dynamics for control design.

2.3 Motor model

To properly evaluate the handling qualities, the dynamics of the electric DC motor must be modelled. The motor-rotor system model is laid out by Malpica and Withrow-Maser [4]. The rotor acceleration is given by

$$I_{\text{rotor}}\dot{\Omega} = K_t i - Q_A - B\Omega, \tag{2}$$

where $K_t i$ represents the motor torque, Q_A represents the aerodynamic torque and $B\Omega$ represents viscous losses. The current of the motor is governed by Equation (3),

$$L\frac{di}{dt} = V - K_e\Omega - R_m i, \tag{3}$$

where L is the motor inductance (usually very small), V is the applied voltage, $K_e\Omega$ represents the back-EMF of the motor ($K_e = K_t$ only if using SI units) and $R_m i$ represents the Ohmic losses across the motor.

Table 1. *Shared aircraft parameters*

Parameter	Value
Gross weight	5,360N
Disk loading	287N/m^2
Total disk area	$5.95\pi m^2$
Rotor root pitch	21.5°
Rotor twist	−10.4°
Tip clearance	0.1R

Table 2. *Varying aircraft parameters*

Parameter	Quad	Hex	Oct
Rotor radius [m]	1.21	1.00	0.86
Boom length [m]	1.81	2.09	2.37
I_{rotor} [kg m^2]	2.01	0.736	0.357
I_{xx} [kg m^2]	466	502	544
I_{yy} [kg m^2]	549	584	625
I_{zz} [kg m^2]	904	975	1060

Table 3. *Motor parameters*

	Quad	Hex	Oct
K$_t$ [Nm/A][a]	1.18	0.79	0.59
R$_m$ [mΩ]	47.5	47.5	47.5

[a]K$_e$ [Vs/rad] is equivalent to K$_t$ if using SI units.

If the inductance of the motor is completely neglected, the electrical dynamics settle instantaneously, and Equation (3) can be solved for the motor current. Substituting the result into Equation (2) and assuming the viscous losses are negligible yields

$$I_{\text{rotor}}\dot{\Omega} = \frac{K_t}{R_m}V - \frac{K_e^2}{R_m}\Omega - Q_A, \tag{4}$$

which is the governing equation for the rotor speed. Using a known rotor thrust, torque, speed and assumed motor efficiency (95%), the motor parameters (K_t and R_m) can be calculated as in Ref. [4], and are tabulated in Table 3.
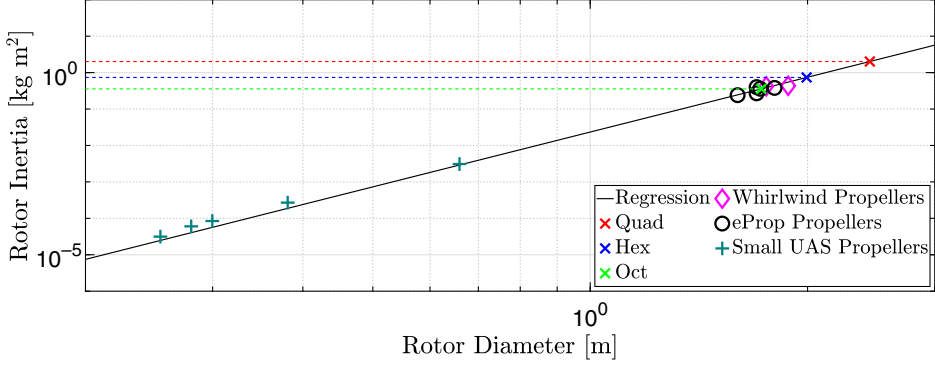
2.4 Rotor inertia

Rotor inertia estimates are based on a regression analysis performed for small UAS rotors by Walter et al. [2], and is given by the expression in Equation (5). The fit is shown in Fig. 4, where the rotors ranging from 0.254 to 0.660m in diameter used by Walter are represented by the plus symbols. To validate the preexisting fit for larger rotors, the regression was compared to rotors in the 1.6 to 1.88m diameter range manufactured by Whirlwind[1] and Eprop[2], represented by the diamonds and the circles, respectively. The fit is excellent in this regime, with $R^2 = 0.9716$, justifying the use of this regression for the rotor inertia of the quadcopter, hexacopter, and octocopter, represented by the "x" symbols in Fig. 4. The rotor inertias are also listed in Table 2.
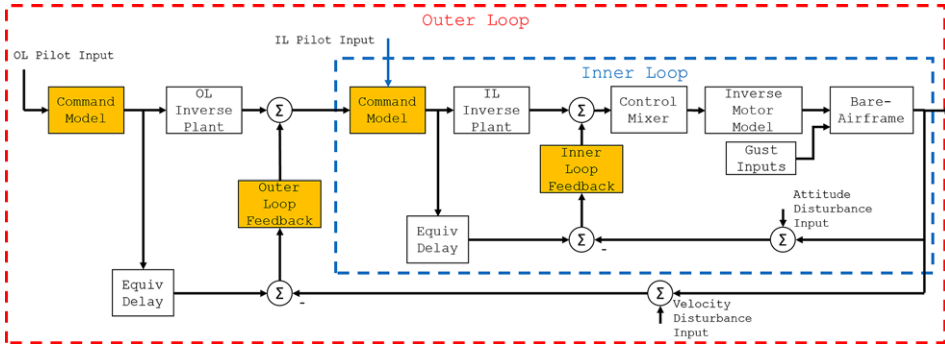
$$I_{\text{rotor}} = 0.7476R^5 \tag{5}$$

---

[1]"Whirlwind Standard Propeller". Viking Aircraft Engines. https://www.vikingaircraftengines.com/new-products/whirlwind-standard-propeller. Accessed Jul. 26, 2020.

[2]"Propeller and Moment of Inertia". The E-Prop Company. https://ppg.e-props.fr/design/#titr09. Accessed Jul. 31, 2020.

Figure 4. *Rotor Inertia with Varying Rotor Size*

Figure 5. *Control System Architecture*

3.0 Control optimisation

A state space model linearised about a trim condition is utilised to design a control system. The control optimisation suite CONDUIT® [6] is used to optimise a controller for actuator effort, while meeting the specifications presented by ADS-33E-PRF [7].

The explicit-model-following control architecture for the multicopters is illustrated in Fig. 5, where the blocks that are tuned during the control optimisation routine are highlighted. The inner loop consists of attitude-command-attitude-hold (ACAH) response-type controllers on the longitudinal and lateral axes (pitch and roll, respectively), along with a rate-command-direction-hold (RCDH) controller in yaw. The longitudinal and lateral axes follow a second order command model and utilise PID feedback controllers, while yaw follows a first order command model and features a PI feedback controller. In this study, both the pitch and roll axes utilise the same second order command model and feedback controller. Based on a desired attitude or yaw rate, the inner loop determines a desired speed for the rotors (in multi-rotor coordinates). After utilising the multi-rotor coordinate transform (Equation (1)) to obtain the desired individual motor speeds, an open-loop controller (based on an inversion of a linearised Equation (4)) is used to determine the voltage delivered to each motor. The specifications used for the inner loop controller are listed in Table 4.

The outer loop consists of translational rate command (TRC) controllers in the longitudinal, lateral and vertical axes. All outer loop axes follow a first order command model and feature PI feedback controllers. For the longitudinal and lateral axes, the outer loop determines a desired pitch and roll attitude, which commands the ACAH controllers in the inner loop. For the vertical axis, the outer loop determines a desired mean rotor speed, which is fed directly to the control mixer. The outer loop specifications are listed in Table 5.

Table 4. *CONDUIT® inner loop Hover specifications*

Specification	Axes
Hard constraints	
Eigenvalues	All
Stability margins	Roll, Pitch, Yaw
Nichols margins	Roll, Pitch, Yaw
Soft constraints	
Bandwidth	Roll, Pitch, Yaw
Crossover frequency	Roll, Pitch, Yaw
Disturbance Rej. bandwidth	Roll, Pitch, Yaw
Disturbance Rej. peak	Roll, Pitch, Yaw
Closed loop damping ratio	All
Model following	All
OLOP (Pilot)	Roll, Pitch, Yaw
OLOP (Disturbance)	Roll, Pitch, Yaw
Summed objectives	
Actuator RMS (Pilot)	Roll, Pitch, Yaw
Actuator RMS (Disturbance)	Roll, Pitch, Yaw
Crossover frequency	Roll, Pitch, Yaw

Table 5. *CONDUIT® outer loop Hover specifications*

Specification	Axes
Hard constraints	
Eigenvalues	All
Stability margins (Inner loop)	All
Stability margins (Outer loop)	All
Nichols margins (Inner loop)	All
Nichols margins (Outer loop)	All
Soft constraints	
Crossover frequency	All
Disturbance Rej. bandwidth	All
Disturbance Rej. peak	All
Heave mode	Heave
Closed loop damping ratio	All
Model following	All
OLOP (Pilot)	All
OLOP (Disturbance)	All
Rise time	Longitudinal & Lateral
Summed objectives	
Actuator RMS (Pilot)	All
Actuator RMS (Disturbance)	All
Crossover frequency	All

Table 6. *Control optimisation design parameters*

Design parameter	Axes
Command models	
Command model frequency	Pitch & Roll
Yaw time constant	Yaw
OL time constant	Longitudinal & Lateral
Heave time constant	Heave
Rotor speed time constant	–
Feedback controllers	
IL derivative gain	Pitch & Roll
IL proportional gain	Pitch & Roll
Yaw proportional gain	Yaw
OL proportional gain	Longitudinal & Lateral
Heave proportional gain	Heave

During the optimisation routine, gains in the command models and feedback controllers are tuned to satisfy the hard and soft constraints while minimising the summed objectives. There are three phases in the control optimisation process [6]. Phase 1 tunes the control gains to meet the hard constraints (stability specifications in Tables 4 and 5). During Phase 2, the optimisation process tunes the gains to meet the soft constraints (handling qualities specifications), while still meeting the hard constraints. Once the hard and soft constraints are met the optimisation process moves to Phase 3, where the summed objectives are minimised. Tables 4 and 5 detail the specifications used in each phase. Two different crossover frequency specifications are utilised, as a soft constraint and summed objective. It is necessary to include both of these specifications due to the 2-DOF architecture used [6]. The design parameters that are tuned by CONDUIT® during the optimisation routine are shown in Table 6. The integral gains for the inner and outer loops are scaled from the corresponding proportional gains by a fixed integral ratio. Included in both the inner and outer loops is an Open-Loop-Onset-Point (OLOP [18]) specification. This specification indicates whether a vehicle is susceptible to pilot-induced or limit-cycle oscillations due to actuator rate saturation. In the case of a variable-RPM multicopter, the key limitation is the deliverable current to the motor, which corresponds to a limit in $\dot{\Omega}$. Thus, for the OLOP specifications, a maximum current is assumed using a design parameter, K (in terms of the hover current, the maximum current is $K \times i_{\text{hover}}$). From Equation (2) (neglecting viscous losses), this motor will have a maximum $\dot{\Omega}$ of

$$\dot{\Omega}_{\text{max}} = \frac{K_t (K-1) i_{\text{hover}}}{I_{\text{rotor}}}, \tag{6}$$

which is used for the evaluation of the OLOP specification. By increasing or reducing K until the OLOP specification is on the Level 1/2 boundary, a minimum motor current margin can be identified.

4.0 Results

4.1 Hover trim and performance

The hover performance for all configurations is tabulated in Table 7. In hover only collective RPM is required, as there are no external moments to balance (the vehicle C.G. is assumed to be located at the geometric centre of the aircraft). If the aircraft C.G. and geometric centre are not coincident, then additional control inputs will be required to account for the moment imbalance, primarily changing the aircraft trim. An Ω_{1s} input is needed for a lateral offset of the C.G., and an Ω_{1c} input is needed for a longitudinal offset. As the rotors of the three vehicles all have the same pitch, solidity and airfoil distribution, they have a common C_T. This, combined with the fact that all three vehicles have identical

Table 7. *Hover performance*

	Quad	**Hex**	**Oct**
Ω_0 [rad/s]	114	139	161
Tip speed [m/s]	139	139	139
Rotor thrust [N]	1,343	894	672
Rotor torque [N m]	178	96.4	62.6
Motor power [each, kW]	21.2	14.1	10.6
Motor current [each, A]	150	122	106
Motor voltage [V]	141	115	100
Total vehicle power [kW]	84.8	84.8	84.8
Motor weight fraction[a]	8.6%	7.6%	7.0%

[a]Represents Weight Fraction from Hover Torque Requirement Only, Calculated from Equation (7).

Table 8. *Inner loop handling qualities specifications*

| Parameter	Unit	**Roll**			**Pitch**			**Yaw**		
		Quad	**Hex**	**Oct**	**Quad**	**Hex**	**Oct**	**Quad**	**Hex**	**Oct**
Stability gain margin[a]	dB	14	16	17	13	14	16			
Stability phase margin	deg	48	45	45	49	45	45	109	106	101
Disturbance rejection bandwidth	rad/s	1.18	1.29	1.36	1.16	1.27	1.34	0.97	0.97	0.98
Disturbance rejection peak	dB	2.83	3.22	3.29	3.35	3.66	3.71	0.27	0.24	0.22
Bandwidth	rad/s	2.50	2.50	2.51	2.49	2.5	2.5	1.4	1.4	1.4
Phase delay	ms	90	92	85	84	86	80	2.1	2.0	2.0
Crossover frequency	rad/s	5.7	5.7	5.9	5.0	5.0	5.3	5.0	5.0	5.0
Command model following	–	48	41	29	49	42	30	0.06	0.05	0.06
OLOP magnitude (Pilot)[b]	dB									−3.4
OLOP phase (Pilot)[b]	deg									−69
OLOP magnitude (Disturbance)	dB	−2.9	−3.8	−4.2	−4.3	−5.7	−6.1	0.30	1.75	3.0
OLOP phase (Disturbance)	deg	−136	−140	−140	−137	−142	−142	−72	−80	−88
Actuator RMS (Pilot)	–	0.024	0.026	0.021	0.029	0.026	0.025	0.094	0.13	0.17
Actuator RMS (Disturbance)	–	0.11	0.15	0.14	0.11	0.13	0.14	0.78	1.19	1.62

[a]Blank entry indicates no 180° crossing in relevant frequency range.
[b]Blank entry indicates that rate limit not reached at relevant frequency range.

disk loading, results in the configurations having the same vehicle power and rotor tip speed of 139m/s. Both the nominal voltage and individual motor current scale with $N_{\text{rotors}}^{-1/2}$, which suggests that having more rotors will generally increase vehicle current requirements (scales with $N_{\text{rotors}}^{1/2}$). And hence that, electrical losses (not modelled in this study) may be greater on an octocopter than a quadcopter. To meet hover torque requirements, the quadcopter requires the largest motor weight fraction (8.6%), with the hexacopter (7.6%) and octocopter (7.0%) requiring less.

4.2 Inner loop performance

CONDUIT® was able to achieve Level 1 handling qualities specifications for all three multicopters. The inner loop handling qualities results are tabulated in Table 8. Relevant inner loop handling qualities windows are also presented in Figs 6–11. Specifically, bandwidth and phase delay for roll and pitch,
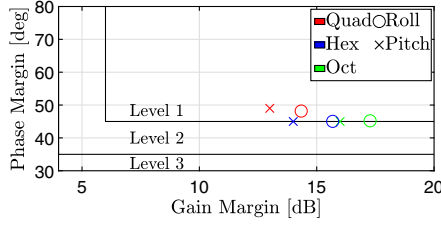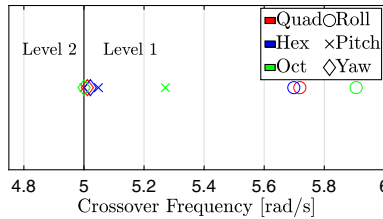
Figure 6. *IL Stability Margins*
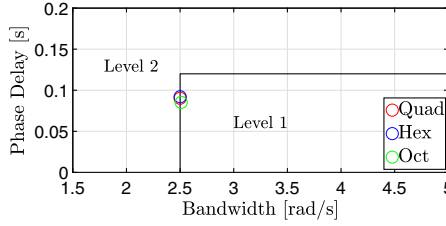
Figure 7. *Roll Bandwidth & Phase Delay*
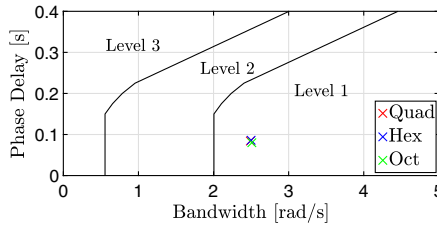
Figure 8. *Pitch Bandwidth & Phase Delay*

Figure 9. *IL Crossover Frequency*

as well as stability margins and crossover frequency for the inner and outer loops are shown. Frequency responses to disturbance inputs are shown in Figs 12 and 13, showing both the disturbance rejection bandwidth and frequency for each configuration (which are also tabulated in Tables 8 and 9). Further, model following frequency responses for each configuration are shown in Figs 14 and 15.

As expected, considering the similarity in the vehicle dynamics, the quadcopter, hexacopter and octocopter achieve similar levels of performance in nearly all of the handing qualities specifications. The phase margin for the hexacopter and octocopter are on the Level 1/2 boundary in both the roll and pitch axes, shown in Fig. 6. All three configurations share a piloted bandwidth of 2.5rad/s in both the roll and pitch axes (Figs 7 and 8), which puts the roll bandwidth on the Level 1/2 boundary (pitch bandwidth is within Level 1). The pitch and roll axes have the same piloted bandwidth due to their shared command model. The only notable exception is the OLOP specification in yaw, which generally gets worse as the number of rotors increases.
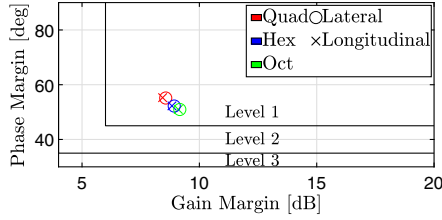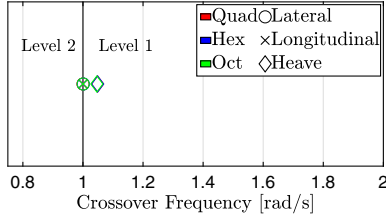
Figure 10. *OL Stability Margins*

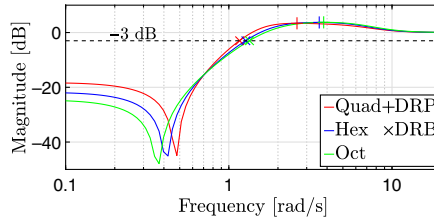**Figure 11.** *OL Crossover Frequency*
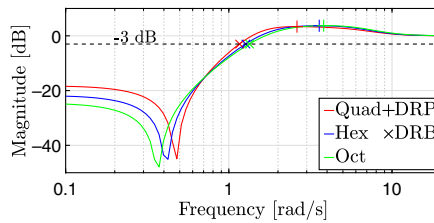

Figure 12. *IL Pitch Disturbance Rejection*

Figure 13. *OL Longitudinal Disturbance Rejection*

Representative disturbance rejection frequency responses for the three configurations are shown in Figs 12 and 13. Both the roll and pitch (inner loop, Table 8) disturbance rejection characteristics are extremely similar and are represented by the pitch disturbance rejection plot, shown in Fig. 12. Similarly, the disturbance rejection response between the longitudinal and lateral axes (outer loop, Table 9) are identical and represented by the longitudinal response, presented in Fig. 13. In all axes, the disturbance rejection response for the three configurations range from being extremely similar, in the case of pitch and roll, to identical, for yaw and all outer loop axes. Therefore, the yaw and heave disturbance rejection plots are not shown, as Table 8 (yaw) and Table 9 (heave) represent the results.

The command model following frequency responses are shown in Figs 14 and 15. In each axis all three configurations follow the same command model, and the three configurations have extremely

Table 9. *Outer loop handling qualities specifications*

| Parameter	Unit	Lateral			Longitudinal			Heave		
		Quad	Hex	Oct	Quad	Hex	Oct	Quad	Hex	Oct
Stability gain margin[a]	dB	8.6	8.9	9.2	8.4	8.8	9.1			
Stability phase margin	deg	55	52	51	55	52	51	87	87	87
Disturbance rejection bandwidth	rad/s	0.61	0.60	0.60	0.60	0.60	0.60	0.5	0.5	0.5
Disturbance rejection peak	dB	5.0	4.9	4.9	5.0	4.9	4.9	0.63	0.63	0.62
Crossover frequency	rad/s	1	1	1	1	1	1	1.05	1.05	1.05
Command model following	–	28.8	15.7	10.3	30.0	16.2	10.6	0.07	0.07	0.07
Heave mode pole	rad/s							0.2	0.2	0.2
Heave mode time delay	ms							89	89	87
Rise time	s	5.0	4.9	4.9	5.0	4.9	4.9			
OLOP magnitude (Pilot)[b]	dB	−71	−88		−31	−76				
OLOP Phase (Pilot)[b]	deg	−322	−337		−280	−328				
OLOP Magnitude (Disturbance)	dB	−5.7	−8.0	−10.2	−5.0	−6.9	−8.8	−3.8	−5.1	−6.2
OLOP Phase (Disturbance)	deg	−160	−174	−187	−155	−167	−178	−98	−99	−101
Actuator RMS (Pilot)	–	0.13	0.14	0.11	0.15	0.14	0.13	0.10	0.080	0.072
Actuator RMS (Disturbance)	–	0.60	0.64	0.50	0.70	0.64	0.57	0.96	0.79	0.72

[a]Blank entry indicates no 180° crossing in relevant frequency range.
[b]Blank entry indicates that rate limit not reached at relevant frequency range.
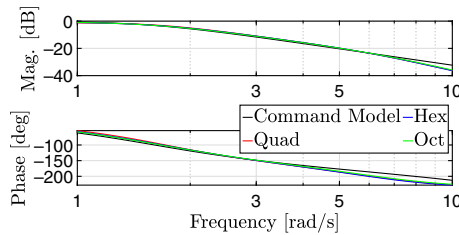
Figure 14. *IL Pitch Model Following*

similar aircraft responses (since they are tuned to the same specifications). Therefore, pitch model following will represent the inner loop (Fig. 14), and the longitudinal model following will represent the outer loop (Fig. 15), and heave (Table 9) and yaw (Table 8) will not be shown, as they have identical cost. The configurations with the largest model following cost, such as the quadcopter in roll and pitch (Fig. 14), have the largest deviation from the command model in the frequency range of interest. Both the longitudinal and lateral axes (inner and outer loop) deviate most from the model at the higher end of the frequency range considered. For the inner loop, the gain deviation occurs above 8rad/s while the phase deviation begins at 5rad/s. The outer loop sees a larger deviation in gain (between 0.7 and 2rad/s, Fig. 15), while the phase is noticeably different between 1 and 2rad/s.

The values reported in Table 8 represent a case where the motor current margin is equal to the current required to hover ($K = 2$). This results in over-performance in the OLOP specifications, suggesting that motor weight reduction is possible without violating any of the handling qualities specifications. The
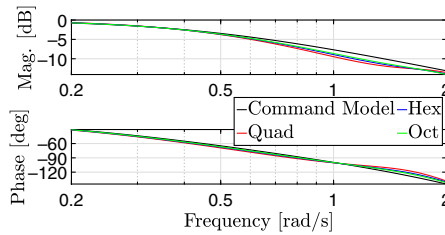
Figure 15. *OL Longitudinal Model Following*

quadcopter and hexacopter reach the Level 1/2 boundary of the OLOP specification with a 53% ($K = 1.53$) motor current margin, limited by roll disturbance input. The octocopter reaches the Level 1/2 boundary at 62% ($K = 1.62$) current margin, limited by a piloted yaw rate input.

For the actuator RMS objective functions in pitch, there are multiple effects to consider. Specifically, the reduced inertia of the rotors reduces the actuator effort required as the rotor radius decreases. In evaluating RMS, the raw inputs are normalised by a reference value derived from the hover voltage (which is lower as more rotors are added). These two effects largely cancel out in pitch, and the RMS specifications are similar.

However, in yaw, the rotor inertia has no effect on the actuator activity level. This is because the reaction torque experienced by the aircraft is directly dependent on the motor torque/current. Whether that torque is used to accelerate the rotor, or overcome aerodynamic drag is irrelevant—the effect on the aircraft is the same. However, the normalisation still occurs, which results in higher RMS as the number of rotors increases.

4.3 Inner loop time simulation

As another means of determining the current requirements for manoeuvre, several time-domain simulations were run. To examine the behaviour under piloted inputs, doublet and step commands were given to the inner loop. For disturbance analysis, 1-cosine gusts were applied [19]. The gust duration is determined by the frequency which maximises the motor current due to a gust input, shown on the Bode plot in Fig. 16. The three configurations share a frequency (6.3rad/s, 1s period) which maximises motor current. The magnitude of piloted and gust inputs is equal to the maximum input used to evaluate the OLOP specification. For both types of inputs, the motor current response of all three vehicles were examined.

4.3.1 Longitudinal axis

The longitudinal and lateral dynamics are qualitatively similar on multicopters, due to the symmetry of the configuration. The only difference between the two is that the pitch inertia is slightly greater than the roll inertia. Thus, the longitudinal axis will require greater effort to control, and is presented here.

A $10°$ pitch doublet is used as pilot input and is plotted along with the filtered commands and the closed-loop response of the vehicle in Fig. 17. All three vehicles respond similarly, as expected, since they were all tuned to the same closed-loop requirements. The octocopter follows the command with the least error, followed by the hexacopter and quadcopter.

Figure 18 shows the current change required by the most longitudinally extreme rotors on the quadcopter, hexacopter and octocopter (Motor 1 for all three, Figs 1–3). The current is normalised by the current required to hover in Table 7, this normalisation represents a relative current margin required to execute the manoeuvre. All three curves are characterised by large current spikes when the pitch command goes through a step change. When this occurs, the desired motor speeds change rapidly, requiring a surge in motor torque/current. The quadcopter requires the greatest margin (33.4%), followed
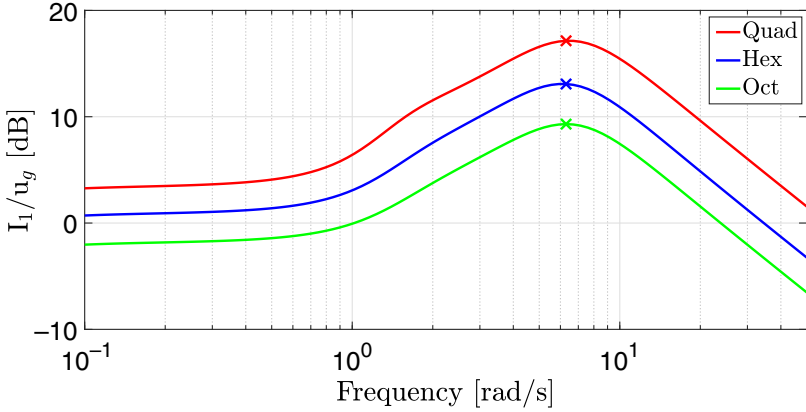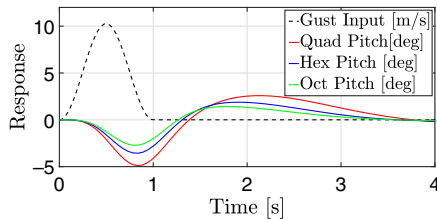
Figure 16. *Frequency Response of Longitudinal Gust to Motor 1 Current*
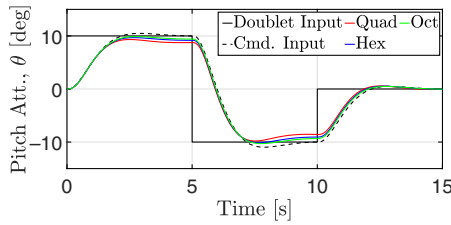
Figure 17. *Pitch Doublet Input and Vehicle Response*
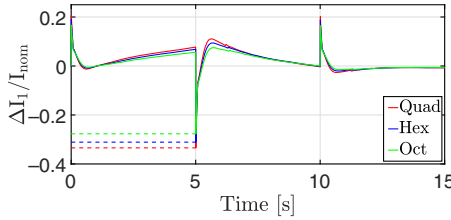
Figure 18. *Motor 1 Normalised Current Response to Pitch Doublet Input*

Figure 19. *Longitudinal Gust Input and Pitch Response*

by the hexacopter (31%) and octocopter (27.7%), as the smaller rotors have less rotational inertia to overcome.

The response of the vehicles to a 10m/s 1-cosine [19] longitudinal gust (applied as a tailwind) is shown in Fig. 19. As the aircraft experience a tailwind, they initially pitch nose-down (due to a positive M_u), and the feedback controller reacts to stabilise the vehicle and return it to a nose-level condition.
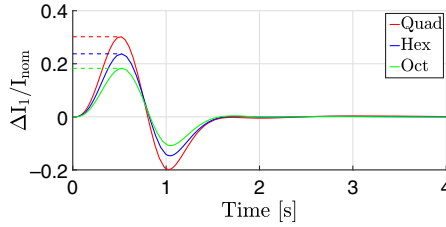
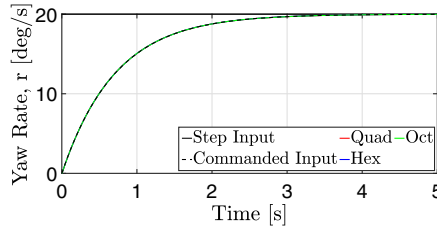**Figure 20.** *Motor 1 Normalised Current Response to Longitudinal Gust*

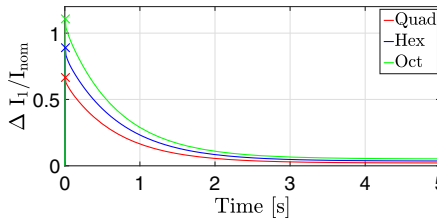**Figure 21.** *Yaw Rate Input and Vehicle Response*

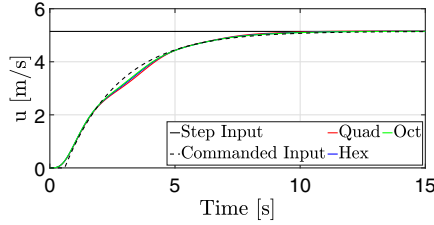**Figure 22.** *Motor 1 Normalised Current Response to Yaw Rate Input*

The maximum nose-down deflection is around 5 degrees and is slightly reduced as the number of rotors increases. The current delivered to the front-right rotor is plotted in Fig. 20, again normalised by the hover current of each individual aircraft. Naturally, the current supplied to this rotor is positive initially, as the aircraft tries to produce a nose-up moment to counteract the effect of the gust. The quadcopter requires the greatest current margin of all three configurations, due to the greater inertia of its rotors.

Rejecting a 10m/s gust requires less current than following the 10° doublet command for all configurations. The quadcopter requires 30% current margin to reject the gust, while the hexacopter and octocopter require 24% and 18% current margin, respectively. The quadcopter has comparable current margin when rejecting the gust or following the doublet command, requiring only 3% less than the doublet. This difference is more pronounced as the number of rotors increases, with the hexacopter and octocopter having an 8% and 10% lower current requirement for gust rejection, respectively.

4.3.2 Yaw axis

To examine the vehicle response to a piloted input in yaw rate, a 20°/s step command was issued to all three vehicles (Fig. 21). All three vehicles respond identically, as expected, following the first-order command model well.

The current (normalised by the hover current of each individual aircraft) required by the front-right rotor to follow the yaw step is plotted in Fig. 22. At the beginning of the simulation, the desired yaw acceleration is very high, which will require a large surge in the motor torque/current. Importantly, unlike the other axes, the vehicle does not rely on the rotor speed for yaw moment, so the primary

Figure 23. *Longitudinal Velocity Input and Vehicle Response*
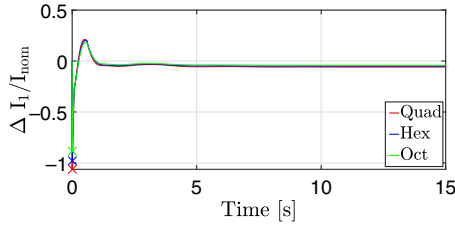
Figure 24. *Motor 1 Normalised Current Response to Longitudinal Velocity Input*

advantage of the octocopter over the quadcopter and hexacopter is gone. In fact, the octocopter requires the greatest current margin of all three configurations, requiring 111% of the hover current margin. The quadcopter and hexacopter require significantly less current margin in this axis, requiring 67% hover and 89% hover current margin, respectively. The octocopter requires the greatest current margin due to it having the greatest yaw inertia (Table 2), which requires more torque to accelerate.

4.4 Outer loop performance

CONDUIT® was also able to achieve Level 1 handling qualities for all three configurations in the outer loop and are tabulated in Table 9. As was the case for pitch in the inner loop, all of the aircraft achieve the same level of performance. With both the longitudinal and vertical axes relying on motor speed change, as the rotors become smaller, there is a decrease in actuator RMS for piloted and disturbance inputs.

4.5 Outer loop time simulations

4.5.1 Longitudinal axis

The aircraft and motor 1 current response to a 5m/s longitudinal velocity step command is shown in Figs 23 and 24, respectively. The response of all three configurations is nearly identical, as expected. Similar to pitch in ACAH mode, as the number of rotors increases, the required current to each motor decreases. For all three configurations, the required current is significantly greater for this input than the 10° doublet command. This increase in current is due to a higher pitch command model frequency, which is necessary to meet minimum phase margin requirements in the outer loop. The quadcopter requires 106% of its hovering current, and the hexacopter and octocopter require slightly less current margin, needing 98% and 88% of hover current, respectively.

A 1-cosine gust with a 1s duration (dashed black line in Fig. 25) was applied to all three configurations. For all three aircraft, the tailwind causes the aircraft to drift forward, and the feedback controller returns it to a steady hover within 4s after the end of the gust. The current (Fig. 26) follows a similar trend to the ACAH response-type, with the quadcopter requiring about 32% current margin to reject the gust, while the hexacopter and octocopter require 25% and 19% current margin, respectively. This current margin is similar to the inner loop gust rejection requirements, and is much less than is required during the step command in velocity.
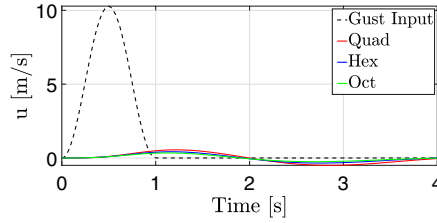
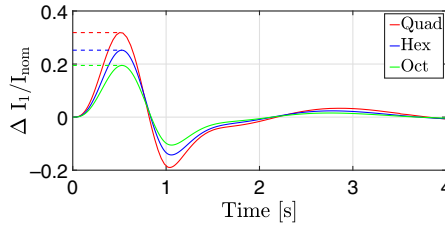**Figure 25.** *Longitudinal Gust Input Outer Loop Response*

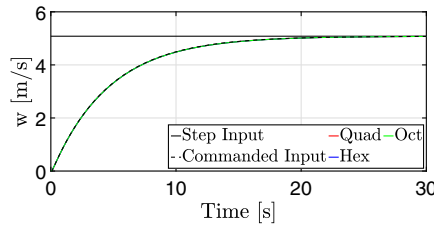**Figure 26.** *Motor 1 Current Response to Longitudinal Gust*

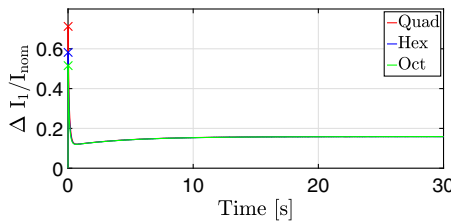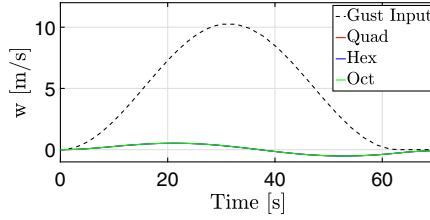**Figure 27.** *Heave Step Input and Vehicle Response*

Figure 28. *Motor 1 Normalised Current Response to Heave Step*

*4.5.2 Heave axis*

A 5m/s climb rate is commanded to all three multicopters in Fig. 27. As expected from the identical handling qualities specifications, all three vehicles follow the same trajectory. Since heave control relies on the rotor thrust (and thus speed), similar trends with the longitudinal axis are observed in the motor current, plotted in Fig. 28. The quadcopter requires the greatest current margin (71%), while the hexacopter (58%) and octocopter (52%) require less.

Similar to the longitudinal axis, a 10m/s magnitude 1-cosine downdraft was applied to the vertical axis of all three configurations. The frequency for this gust (0.1rad/s, 63s duration) was chosen to maximise the motor current. All three aircraft have the same response to the vertical gust, reaching a 0.5m/s peak magnitude heave response shown in Fig. 29. All three configurations also utilise the same normalised current to reject the gust, requiring 25% of hover current shown in Fig. 30. All three vehicles behave identically due to the quasi-steady behaviour of the gust.
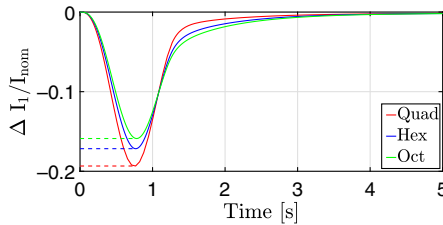
Figure 29. *Heave Gust and Vehicle Response*
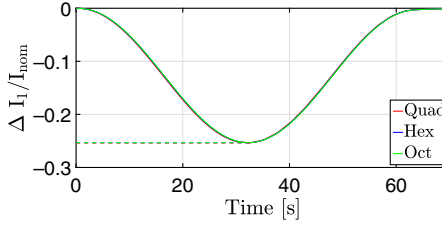
Figure 30. *Motor 1 Normalised Current Response to Heave Gust*
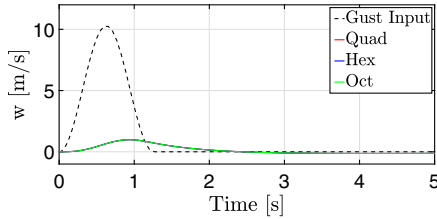
Figure 31. *Quick Heave Gust Input and Response*

Figure 32. *Motor 1 Normalised Current Response to Quick Heave Gust*

The effect of the rotor inertia can be observed for higher-frequency gusts. A 10m/s magnitude, 1.26s duration (5rad/s frequency) gust is applied to the vertical axis of all three configurations in Fig. 31, while the required motor current is shown in Fig. 32. All three configurations respond identically to the gust, reaching a descent heave rate of nearly 1 m/s. The quadcopter requires the highest current margin, needing 19% hover current, while the hexacopter and octocopter require 17% and 16% hover current, respectively.

4.6 Motor weight

An estimation for motor weight can be made based on the peak current across all manoeuvres for each configuration. The peak motor torque is determined by the product of the motor torque constant and peak current. This peak motor torque can then be related to a motor weight using Equation [7], with

Table 10. *Maximum Current & Motor Weight, With Outer-Loop TRC*

Configuration	Manoeuvre	Maximum Current (A)	Maximum Torque (N m)	Motor Weight (kg, each)	Weight Fraction (%)
Quadcopter	Longitudinal Velocity Step	310	366	21.8	15.9
Hexacopter	Longitudinal Velocity Step	243	191	12.5	13.7
Octocopter	Yaw Rate Step	224	132	9.1	13.3

Table 11. *Maximum Current & Motor Weight, Without Outer-Loop TRC*

Configuration	Manoeuvre	Maximum Current (A)	Maximum Torque (N m)	Motor Weight (kg, each)	Weight Fraction (%)
Quadcopter	Heave Step	257	304	18.6	13.6
Hexacopter	Yaw Rate Step	232	183	12.0	13.2
Octocopter	Yaw Rate Step	224	132	9.1	13.3

torque in ft-lb and resulting motor weight in lb.

$$W_{eng} = 0.3928 Q^{0.8587} \qquad (7)$$

The limiting case for each configuration and the resulting motor weight is summarised in Table 10. Both the quadcopter and hexacopter are limited by a longitudinal velocity command, while the octocopter is limited by a yaw rate command. The quadcopter requires individual motors that are more than 9 kg heavier than the hexacopter or octocopter. The hexacopter and octocopter have roughly the same motor weight fraction (of about 13.5%), while the quadcopter is about 16%. Compared to hover requirements (Table 7), the quadcopter requires an additional 7.3% motor weight fraction to meet handling qualities requirements, while the hexacopter and octocopter require an additional 6.1% and 6.3%, respectively.

The difference in motor weight fraction between the configurations will lead to improvement in hover performance. The difference in motor weight fraction between the quadcopter and hexacopter (2.2%), for example, allows for an additional 12kg of batteries (improving range and endurance) or additional payload. While the octocopter (2.6% motor weight fraction difference) is capable of carrying an additional 14.2kg of payload or battery. Assuming a battery energy density of 200Wh/kg, the reduction in motor weight fraction provides an additional 102s of hover endurance for the hexacopter and an additional 121s for the octocopter.

If the longitudinal and lateral axes are flown exclusively in ACAH mode, the limiting cases for the quadcopter and hexacopter become heave and yaw rate step commands, respectively. The current margin and motor weight are summarised in Table 11. The only vehicle to see any substantial reduction in the required motor weight is the quadcopter, which is now similar to the hexacopter and octocopter. The latter two configurations may further benefit from the introduction of rotor cant, which can reduce the current required to yaw the vehicle by reorienting rotor thrust to produce a direct yaw moment [5]. However, this comes at the cost of increasing the rotor thrust needed to regulate the other axes, so the quadcopter cannot benefit in the same way.

5.0 Conclusion

Optimisation-based control design techniques were applied to a 5,360N gross weight quadcopter, hexacopter and octocopter with variable-RPM rotors, and the handling qualities and relative motor

requirements were compared in hover at 287N/m^2 disk loading. When held to the same handling qualities requirements, all three configurations follow commands and reject disturbances identically to one another.

In axes that are regulated by rotor thrust, namely, pitch, roll and heave, configurations with more rotors required less current margin than similarly sized vehicles with fewer, larger rotors. This is due to the fact that, in order to change thrust on a variable-RPM vehicle, the rotor's inertia must be overcome. Both the quadcopter and hexacopter were limited in axes that are regulated by rotor thrust. A step command in longitudinal velocity required 106% and 98% of hover current for the quadcopter and hexacopter, respectively.

In yaw, the dependence is directly on motor current, as the motor reaction torque (regardless of whether the motor is overcoming aerodynamic drag or accelerating the rotor) is what controls the aircraft. Because the octocopter has slightly more inertia in yaw (longer booms are needed to maintain rotor tip clearance), the octocopter requires the greatest current (111% of the hover current) of all three configurations to follow a yaw rate step command.

By utilising the relationship between motor torque and weight, an estimate for motor weight necessary to manoeuvre the aircraft to ADS-33E-PRF standards was obtained. The limiting cases for the quadcopter and hexacopter were a step command in longitudinal velocity, while the yaw rate step command was limiting for the octocopter. If only hover torque requirements are considered, the motors represent an 7–9% weight fraction. When handling qualities requirements (with translational rate command) are considered, the motors represent a 13–16% weight fraction. To meet handling qualities requirements, the quadcopter's motors collectively weigh 13.6 kg (approximately 2.5% of the aircraft weight) more than the motors of the hexacopter or octocopter.

References

[1] Antcliff, K., Whiteside, S., Kohlman, L. and Silva, C. Baseline assumptions and future research areas for urban air mobility vehicles, AIAA SciTech *Forum*, San Diego, CA, USA, 2019.

[2] Walter, A., McKay, M., Niemiec, R. and Gandhi, F. An assessment of heave response dynamics for electrically driven rotors of increasing diameter, 8th Biennial Autonomous VTOL Techinical Meeting 6th Annual Electric VTOL Symposium, Mesa, AZ, USA, 2019.

[3] Walter, A., McKay, M., Niemiec, R., Gandhi, F. and Ivler, C. Handling qualities based assessment of scalability for variable-RPM electric multi-rotor aircraft, Vertical Flight Society 75th Annual Forum, Philidelphia, PA, USA, 2019.

[4] Malpica, C. and Withrow-Maser, S. Handling qualities analysis of blade pitch and rotor speed controlled eVTOL quadrotor concepts for urban air mobility, VFS International Powered Lift Converence, San Jose, CA, USA, 2020.

[5] Niemiec, R., Gandhi, F., Lopez, M. and Tischler, M. System identification and handling qualities predictions of an eVTOL urban air mobility aircraft using modern flight control methods, Vertical Flight Society 76th Annual Forum, Virtual, 2020.

[6] Tischler, M., Berger, T., Ivler, C., Mohammadreza, M.H., Cheung, K.K. and Soong, J.Y. Practical methods for aircraft and rotorcraft flight control design: An optimization-based approach, AIAA Education Series, Reston, VA, USA, 2017, doi: 10.2514/4.104435

[7] Aeronautical Design Standard, Performance Specifications, Handling Qualities Requirements for Military Rotorcraft, Technical Report ADS-33E-PRF, 2000.

[8] Ivler, C. and Tischler, M. Case studies of system identification modeling for flight control design, *J. Am. Helicopter Soc.*, January 2013, **58**, (1), pp 1–16, doi: 10.4050/JAHS.58.012003

[9] Wei, W., Tischler, M.B. and Cohen, K. System identification and controller optimization of a quadrotor unmanned aerial vehicle in Hover, *J. Am. Helicopter Soc.*, 2017, **62**, (4), pp 1–9, doi: 10.4050/JAHS.62.042007

[10] Cheung, K., Wagster, J., Tischler, M., Ivler, C., Berrios, M., Berger, T., Juhasz, O., Tobias, E., Goerzen, C., Barone, P., Sanders, F. Lopez, M. and Lehmann, R. An overview of the U.S. Army aviation development directorate quadrotor guidance, navigation, and control project, 2017.

[11] Lopez, M., Tischler, M., Juhasz, O., Gong, A., Sanders, F., Soong, J. and Nadell, S. Flight test comparison of gust rejection capability for various multirotor configurations, Vertical Flight Society 75th Annual *Forum*, Philadelphia, PA, USA, 2019.

[12] Niemiec, R. and Gandhi, F. Multi-rotor coordinate transforms for orthogonal primary and redundant control modes for regualr hexacopters and octocopters, 42nd Annual European Rotorcraft Forum, Lille, France, 2016.

[13] Silva, C., Johnson, W., Antcliff, K. and Patterson, M. VTOL urban air mobility concept vehicles for technology development, Aviation Technology, Integration, and Operations Conference, Atlanta, GA, USA, 2018, doi: 10.2514/6.2018-3847

[14] Niemiec, R. and Gandhi, F. Development and validation of the rensselaer multicopter analysis code (RMAC): A physics-based comprehensive modeling tool, Vertical Flight Society 75th Annual *Forum*, Philadelphia, PA, USA, 2019.

[15] Peters, D., Boyd, D. and He, C.J. Finite-state induced-flow model for rotors in Hover and forward flight, *J. Am. Helicopter Soc.*, 1989, 34, (4), pp 5–17, doi: 10.4050/JAHS.34.5

[16] Ivler, C., Niemiec, R. and Gandhi, F. Multirotor electric aerial vehicle model validation with flight data: Physics-based and system identification models, Vertical Flight Society 75th Annual Forum, Philidelphia, PA, USA, 2019.

[17] Russell, C., Jung, J., Willink, G. and Glasner, B. Wind tunnel and Hover performance test results for multicopter UAS vehicles, American Helicopter Society 72nd Annual Forum, West Palm Beach, FL, USA, 2016.

[18] Duda, H. Flight control system design considering rate saturation, *Aerosp. Sci. Technol.*, 1998, **4**, pp 265–275, doi: 10.1016/S1270-9638(98)80004-7

[19] Berrios, M., Berger, T., Tischler, M., Juhasz, O. and Sanders, F. Hover flight control design for UAS using performance-based disturbance rejections requirements, Vertical Flight Society 73rd Annual *Forum*, Fort Worth, TX, USA, 2017.

[20] Johnson, W. NDARC-NASA design and analysis of Rotorcraft, Technical Report NASA TP 218751, April 2015.